

A limit on top quark pair production at future electron-proton colliders

G. R. Boroun*

Department of physics, Razi University, Kermanshah 67149, Iran

(Dated: February 24, 2026)

The ratio of the structure functions for deep inelastic scattering in top pair production at future electron-proton colliders is analyzed at a fixed \sqrt{s} and Q^2 relative to the minimum value of x given by Q^2/s using collinear factorization. This compact formula for the ratio $F_{L2}(Q^2/s, Q^2, m_t)$ is useful for extracting a bound on the top structure function. The reduced cross-section for top production at this limit is determined, establishing a bound value for $t\bar{t}$ production at the LHeC and FCC-eh center-of-mass energies based on renormalization scales. The modification of the Bjorken scaling is applied to this bound of the reduced top cross-section at the renormalization scale $\mu^2 = Q^2 + 4m_t^2$, which improves the scaling quantity at $Q^2 < 4m_t^2$. The dipole cross-section for top pair production is examined across a wide range of dipole sizes, denoted as r . It is expected that there will be limited behavior in observing top saturation in future electron-proton colliders according to the bound behavior. The probability of the Higgs boson in γ^*g interactions is compared to the gg process at the order of $\mathcal{O}(\alpha^{\text{em}}/\alpha_s)$.

I. INTRODUCTION

One of the main physics goals of the Large Hadron Electron Collider (LHeC) and the Future Circular Collider Electron-Hadron (FCC-eh) is to search for the top quark [1]. These new colliders, namely LHeC and FCC-eh, increase the center-of-mass energy. At the LHeC, it can reach approximately $\sqrt{s} \simeq 1.3$ TeV and at the FCC-eh, it would reach $\sqrt{s} = 3.5$ TeV with a similar luminosity as the LHeC. The kinematic range in the LHeC for electron and positron neutral-current (NC) interactions in the perturbative region is well below $x \simeq 10^{-6}$ and extends up to $Q \simeq 1$ TeV. This range will be extended down to $x \simeq 10^{-7}$ at the FCC-eh option of a Future Circular Collider program [2, 3]. The top cross section can be measured through the boson-gluon fusion (BGF) process which allows for a deeper understanding of the hadronic structure at high energies through deep inelastic scattering (DIS). One of the important production modes for top quarks at the LHeC is photoproduction of top-antitop quark pairs ($t\bar{t}$), for which a total cross-section of 0.05 pb is expected at the LHeC. The LHeC and FCC-eh colliders will create new research opportunities with top cross sections that could not be observed at HERA. The total cross section in DIS for top quark pair production is approximately 53 fb at the LHeC and about 1 pb at the FCC-eh [4].

The top quark is produced in nuclear collisions by gluon-gluon fusion¹ (GGF) [5–8], $g + g \rightarrow t + \bar{t}$, at the LHC. The top quark pair production cross sections are $\sigma_{t\bar{t}} = 984.5$ pb at $\sqrt{s} = 14$ TeV and $\sigma_{t\bar{t}} = 826.4$ pb at $\sqrt{s} = 13$ TeV at CMS [9] and ATLAS [10]. Top quark pair production at the LHC is characterized by final states comprising the decay products of the two W bosons and two b jets, where the $\sigma_{tot}^{t\bar{t}}$ at ultra-high energies for $\mu = m_t$ can be written as [6]

$$\hat{\sigma}_{gg}(\beta, m_t) = \frac{\alpha_s^2}{m_t^2} \{f_{gg}^{(0)} + \alpha_s f_{gg}^{(1)} + \alpha_s^2 f_{gg}^{(2)} + \mathcal{O}(\alpha_s^3)\}. \quad (1)$$

The functions f_{gg} are known at leading and high-order approximations and depend only on dimensionless parameters β and ρ , where $\beta^2 = 1 - \rho$ with $\rho = 4m_t^2/s$ as the squared relative velocity of the final state top quarks having pole mass m_t and produced at the square of the gluonic center of mass energy s .

*Electronic address: boroun@razi.ac.ir

¹ Neutral current (NC) top quark production occurs in both the DIS and photoproduction modes, where single top and top pair production take place, respectively. In the LHeC, a combination of a 60 GeV electron beam and a 7 TeV proton beam from the Large Hadron Collider (LHC), the DIS top pair cross section is approximately 23 fb, which is lower than at the LHC, but offers better measurement potential [4]. In the LHC, any heavy s -channel resonance with a significant branching ratio to $t\bar{t}$ is introduced by the processes $gg \rightarrow t\bar{t}$, where %15 of the contributions to $t\bar{t}$ production come from these processes. One of the production modes for top quarks at the LHeC is the process $\gamma^*g \rightarrow t\bar{t}$, which will explore the strange density and momentum fraction carried by top quarks, something that was previously impossible at HERA.

The study of production mechanisms of top pair quarks provides us with new tests of quantum chromodynamics (QCD) such as Higgs bosons in $t\bar{t}$ production. The top quark has a large Yukawa coupling with the Higgs boson. In the usual extensions of the standard model the Higgs sector includes extra scalars, which also tend to couple strongly with the top quark. This production which is a crucial process at the LHC is studied in Refs.[11–14]. This means that the top quark with a mass of about 172.5 ± 0.5 GeV, measured by ATLAS [10] and CMS [9], and a particle that most strongly influences the Higgs boson and its potential is special among all quarks and can be considered at future colliders. The observed effects of the $t\bar{t}$ productions at the LHC are implemented on the CT18 parton distribution functions (PDFs) recently in [15].

Several methods have been proposed for determining the top structure functions in the DIS that are relevant for investigating ultra-high energy processes, such as the scattering of cosmic neutrinos from hadrons [16–20]. The interaction Lagrangian density due to the electromagnetic coupling in $ep\rightarrow t\bar{t}X$ pair production [19, 20] is defined by the following equation:

$$\mathcal{L}_{em} = -\sqrt{4\pi\alpha_{em}} \left[e_e \bar{\Psi}_e \gamma^\mu \Psi_e + e_t \bar{\Psi}_t \gamma^\mu \Psi_t \right] A_\mu. \quad (2)$$

Here, the Dirac fields Ψ_e , Ψ_t , and the vector field A_μ describe the electron, the top and the photon, respectively. e_e and e_t represent the electric charge of the electron and top-quark in units of $\sqrt{4\pi\alpha_{em}}$, where α_{em} is the fine structure constant. According to the Weizsäcker-Williams² approximation [21–23], the total cross-section for large values of \sqrt{s} is provided by the equation:

$$\sigma = \int_{y_{\min}}^1 dy P_\gamma(y) \int_{z_{\min}}^1 dz x g(z, \mu_F) \hat{\sigma}. \quad (3)$$

Here, P_γ is the photon-splitting function and $\hat{\sigma}$ is the cross section of the $t\bar{t}$ pair production by a real photon, where $z_{\min} = \mu^2/(ys)$. The corresponding hadron-level cross sections, $\sigma_{k=2,L}^t$ in accordance with the WW approximation in the fixed-flavor-number scheme (FFNS), are defined by the following form [19, 20, 24]

$$\sigma_k^t = \int_{z_{\min}}^1 dz G(z, \mu_F) \hat{\sigma}_{k,g}^t\left(\frac{x}{z}, \mu_F, \mu_R\right), \quad (4)$$

where $\hat{\sigma}_{k,g}^t$, ($k = 2, L$) are the γ^*g cross sections of the photon -gluon component of the heavy-quark leptonproduction at the LO approximation, given by:

$$\gamma^* + g \rightarrow t + \bar{t}.$$

Here, μ_R and μ_F are the renormalization and factorization scales, respectively. The default renormalisation and factorization scales are set to be equal $\mu_R^2 = Q^2 + 4m_t^2$ and $\mu_F^2 = Q^2$. The leptonproduction cross sections $\sigma_{k=2,L}^t(x, Q^2)$ are related to the DIS structure functions $F_k^t(x, Q^2)$.

The number of active flavors changes as the scale is increased, therefore parton distributions are released in a variable-flavor- number scheme (VFNS). Usually, $n_f = 5$ is taken as the maximum number of flavors by default. However, in NNPDF [25], $n_f = 6$ PDF sets are also made available. This is important in the running of α_s for precision phenomenology, as the values of α_s with five and six active flavors already differ by about 2% at the TeV scale [26]. Investigations into the top quark structure inside the proton are also discussed in [1, 18, 27, 28].

The total longitudinal and transverse cross sections in the processes of top quark production in DIS via the one-photon exchange mechanism are related to the corresponding DIS structure functions as

$$\begin{aligned} \sigma_L^t(x, Q^2) &= \frac{4\pi^2\alpha_{em}}{Q^2} F_L^t(x, Q^2), \\ \sigma_T^t(x, Q^2) &= \frac{8\pi^2\alpha_{em}}{Q^2} x F_1^t(x, Q^2). \end{aligned} \quad (5)$$

² The Weizsäcker-Williams (WW) approximation is a useful form of approximation for the exact total cross-section for large values of \sqrt{s} . In this approximation, the production rate is described by a convolution of the probability for emitting a photon from the electron with the corresponding real photon cross section for the reaction $\gamma g \rightarrow t\bar{t}$ [20].

Instead of measuring F_1 , experimentalists measure the structure function as [29]

$$F_2^t(x, Q^2) = 2xF_1^t(x, Q^2) + F_L^t(x, Q^2). \quad (6)$$

The reduced cross-section for pair production of top quarks in ep-collisions is defined in terms of the top quark structure functions as

$$\sigma_r^t(x, Q^2) = F_2^t(x, Q^2) - f(y)F_L^t(x, Q^2), \quad (7)$$

where $f(y) = y^2/1 + (1-y)^2$ and y represents the inelasticity. In the collinear generalized double asymptotic scaling (DAS) [30–32] approach, the top quark structure functions are driven at small x by gluons as

$$F_k^t(x, Q^2) = e_t^2 \sum_{n=0} a_s^{n+1}(Q^2) B_{k,g}^{(n)}(x, a) \otimes xg(x, Q^2), \quad (k = 2, L), \quad (8)$$

where $a = m_t^2/Q^2$ and $a_s(Q^2) = \alpha_s(Q^2)/4\pi$. The \otimes symbol denotes the convolution integral, which simplifies to a multiplication in Mellin N -space. The notation is given by $a(x) \otimes b(x) = \int_x^1 \frac{dz}{z} a(z)b(\frac{x}{z})$ and $xg(x, Q^2)$ represents the gluon distribution function. The coefficient functions at the Born level (first order in α_s) and the order α_s^2 contributions are reported in Refs.[33–35]. In order to address the unphysical mass scale μ , the renormalisation and factorisation scale for the heavy quarks is defined as $\mu^2 = Q^2$ and $\mu^2 = Q^2 + 4m_t^2$.

In this work, the collinear approach calculation of top quark pair production at the FCC-he and the LHeC kinematic regions is presented. The focus is on the limited behavior of the reduced cross section of top quark-pair production in the high inelasticity region. The parametrization of gluon distribution and dipole cross-section at the limit $x_{\min} = Q^2/s$ is included. The probability of the production of the Higgs boson from the pair top production in the γ^*g domain of the ep new colliders is defined. The rest of this paper is organized as follows. In Sec. II, the theoretical framework for the coefficient function in the collinear approach is presented. In Sec. III, the numerical results for the reduced cross section $\sigma_r^{t\bar{t}}(Q^2/s, Q^2)$ and for the dipole cross section $\sigma_{\text{dip}}^{t\bar{t}}(Q^2/s, Q^2)$ at ultra-high energy processes are studied.

II. Theory

The top reduced cross-section, as given by Eq. (7), can be rewritten in the following form in the limit $y = 1$

$$\lim_{y \rightarrow 1} \left[\frac{\sigma_r^t(Q^2/s, Q^2)}{F_2^t(Q^2/s, Q^2)} \right] = 1 - \frac{F_L^t(Q^2/s, Q^2)}{F_2^t(Q^2/s, Q^2)}, \quad (9)$$

where $f(y) = 1$ is defined at a fixed \sqrt{s} and Q^2 , and $x_{\min} = Q^2/s$ dominates in nucleons and nuclei. This limit indicates that the longitudinal polarization of the virtual photon at $y = 1$ approaches zero [36, 37]. The ratio of the DIS top structure functions corresponding to $x_{\min} = Q^2/s$ is defined by the following formula:

$$F_{L2}^t(Q^2/s, Q^2) = \frac{F_L^t(Q^2/s, Q^2)}{F_2^t(Q^2/s, Q^2)} = \frac{\sum_{n=0} a_s^{n+1}(\mu^2) B_{L,g}^{(n)}(Q^2/s, a) \otimes xg(Q^2/s, Q^2)}{\sum_{n=0} a_s^{n+1}(\mu^2) B_{2,g}^{(n)}(Q^2/s, a) \otimes xg(Q^2/s, Q^2)}. \quad (10)$$

In the collinear generalized DAS approaches, the coefficient functions $B_{k,g}^{(n)}$ are known but the gluon distribution functions have to be obtained from the Parton Distribution Function groups. One can obtain a non-trivial upper bound on the ratio F_{L2}^t at the limit $y = 1$, which will be valid with new data at the LHeC [1, 27] and EIC [38].

We first consider the bound for the ratio F_{L2}^t as we define [39, 40]

$$g(Q^2, s, m_t) = \frac{\sum_{n=0} a_s^{n+1}(\mu^2) B_{L,g}^{(n)}(Q^2/s, a)}{\sum_{n=0} a_s^{n+1}(\mu^2) B_{2,g}^{(n)}(Q^2/s, a)} = \frac{a_s^1(\mu^2) B_{L,g}^{(0)}(Q^2/s, a) + a_s^2(\mu^2) B_{L,g}^{(1)}(Q^2/s, a) + \dots}{a_s^1(\mu^2) B_{2,g}^{(0)}(Q^2/s, a) + a_s^2(\mu^2) B_{2,g}^{(1)}(Q^2/s, a) + \dots}. \quad (11)$$

In Fig.1, the ratio $g(Q^2, s, m_t)$ is shown at the LO and NLO approximations due to the coefficients $n = 0$ and $n = 1$ in Eq. (11), respectively. In this figure we observe that the results at the LO approximation have a bound limit for the LHeC and FCC center-of-mass (COM) energies. The results for the LHeC and FCC COM energies are very similar at the NLO approximation and increase as Q^2 values increase. Indeed, a bound limit for the DIS top structure

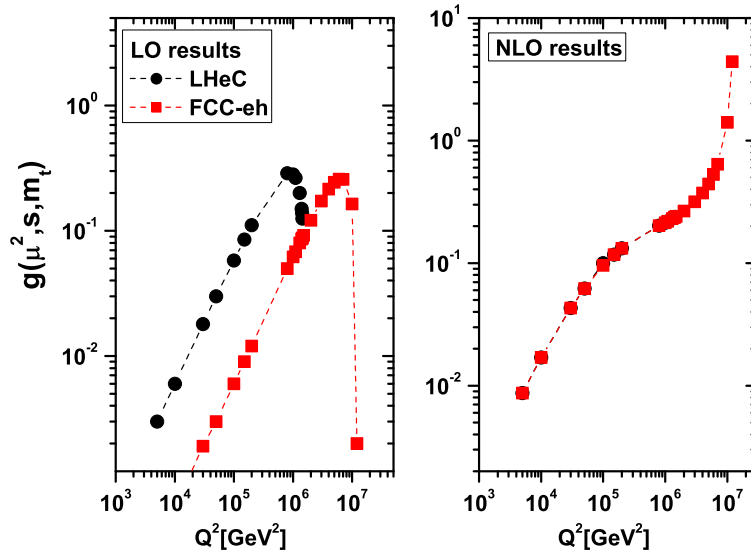


FIG. 1: The function $g(\mu^2, s, m_t)$ is compared versus $\mu^2 = Q^2$ at the LO (left panel) and NLO (right panel) approximations for the LHeC (black circles) and FCC-eh (red squares) colliders with $\sqrt{s} = 1.3$ and 3.5 TeV respectively.

functions is not visible for the LHeC and FCC COM energies using the collinear approximation. Therefore, in the following, we use the LO approximation using collinear factorization.

According to Fig.1, we observe that the function $g(Q^2, s, m_t)$ has a maximum at the LO approximation with ≈ 0.288 and ≈ 0.259 for the COM energies in the LHeC and FCC-eh colliders. These values are comparable to the bounds in the color dipole model (CDM) [39, 40]. Because, the gluon density has to be non-negative, the bound values lead to the bound of top structure functions as

$$\frac{F_L}{F_2}(Q^2, s, m_t) \leq 0.259 - 0.288. \quad (12)$$

With respect to the bound of the ratio F_{L2}^t (i.e., Eq. (12)) at high inelasticity (i.e., $y = 1$), the bounds defined in the LHeC and FCC-eh COM energies do not cover the gluon distributions at x_{\min} . Therefore, in the following, we estimate the top reduced cross-section based on the values that support gluon density at low x values.

The integrated gluon distribution function, $xg(x, Q^2)$, is obtained from the unintegrated gluon distribution (UGD) in the proton and nucleus using the correspondence between the color dipole picture and the k_t -factorization formalism in the leading logarithmic approximation [41]. This method covers kinematic ranges relevant for future lepton-hadron colliders like LHeC/FCC-eh [1, 2, 27] and eRHIC [42]. In Ref.[43], an analytical expression for the gluon distribution function up to the saturation scale is defined. The saturation scale marks the transition between the dilute and saturated gluon system. It is defined as $Q_s^2(x) = Q_0^2(x/x_0)^{-\lambda}$ and is valid at moderate Q^2 values. It is interesting to compare the upper bound for the saturation scale from Fit.2 in Table 1 of Ref.[44]. This plot shows the variation of $Q_s^2(x)$ for the LHeC and FCC-eh COM energies across different Q^2 values. In Fig.2, the behavior of the saturation scale at the limit x_{\min} is plotted as $Q_s^2(x_{\min}) = (\frac{\mu^2}{sx_0})^{-\lambda}$ GeV² at the scales $\mu^2 = Q^2$ and $\mu^2 = Q^2 + 4m_t^2$. This plot shows the variation of $Q_s^2(x_{\min})$ for the LHeC and FCC-eh COM energies. As expected one finds that $Q_s^2 \sim 1.61 - 2.63$ GeV² in the low- x region where $x \simeq 0.59 \times 10^{-6}$ and $x \simeq 0.82 \times 10^{-7}$ respectively. Moreover, we have tested the sensitivity of the saturation scale with the top-quark mass at the renormalization scale $\mu^2 = Q^2 + 4m_t^2$, finding a flat behavior for the saturation scale in the region $10 \leq Q^2 < 10^5$ GeV². These findings at $\mu^2 = Q^2$ confirm results at the high inelasticity within the color dipole framework [45].

The UGD in the small- x regime is determined by the following formula³

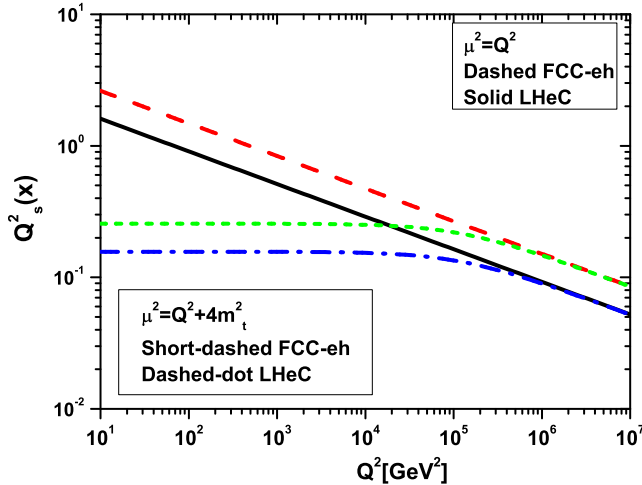


FIG. 2: Saturation scale at x_{\min} is shown at $\mu^2 = Q^2$ and $\mu^2 = Q^2 + 4m_t^2$ for the LHeC and FCC-eh COM energies. LHeC: $\mu^2 = Q^2$ (solid black curve) and $\mu^2 = Q^2 + 4m_t^2$ (dashed-dot blue curve); FCC-eh: $\mu^2 = Q^2$ (dashed red curve) and $\mu^2 = Q^2 + 4m_t^2$ (short-dashed green curve).

$$\alpha_s \mathcal{F}(x, k_t) = \frac{3\sigma_0}{4\pi^2} (k_t^2/Q_s^2) \exp(-k_t^2/Q_s^2). \quad (13)$$

The dipole cross section is related to the UGD through a Fourier transform [49, 50]. Various models [51–55] have been developed to establish the relationship between the UGD and the k_t factorization. The k_t factorization approach to the production of ϕ and ρ mesons in DIS via the helicity-conserving $\gamma^*(T, L) \rightarrow V$ impact factor is discussed in Ref.[56–58]. The results of cross sections for longitudinally and transversely polarized mesons presented at $x_{\min} = Q^2/s$ strongly depend on the choice of UGD. In Fig.3, we plot the k_t^2 dependence of the UGD at $x_{\min} = Q^2/s$ with respect to the LHeC and FCC-eh COM energies. We observe that there is a maximum value for $f(x_{\min}, k_t^2)$ at $\mu^2 = Q^2$ and $\mu^2 = Q^2 + 4m_t^2$. These maximum values increase with increasing Q^2 values when $\mu^2 = Q^2$ is changed to $\mu^2 = Q^2 + 4m_t^2$, and decrease to low k_t^2 as Q^2 increases. An enhancement followed by a depletion in the UGD behavior at $x_{\min} = Q^2/s$ is observable in the LHeC and FCC-eh COM energies with increasing values of k_t [59, 60].

The integrated gluon distribution, as defined by the UGD equation (i.e., Eq. (13)), can be expressed in the following form [43, 60]

$$xg(x, Q^2) = \int_0^{Q^2} dk_t^2 \mathcal{F}(x, k_t) = \frac{3\sigma_0}{4\pi^2 \alpha_s} Q_s^2 \left[1 - \left(1 + \frac{Q^2}{Q_s^2} \right) e^{-\frac{Q^2}{Q_s^2}} \right], \quad (14)$$

where the coefficients of the model are defined in Ref.[44]. The use of the gluon distribution function in heavy quark structure functions in quantum chromodynamics (QCD) is dominant in the fusion reaction $t\bar{t}$ production at high-energy colliders, which is the direct detection of entanglement [61].

³ The relationship between the integrated and unintegrated gluon distribution functions at very low x is defined as follows:

$$f_g(x, k_t^2) \simeq \frac{\partial}{\partial \mu^2} G(x, \mu^2) \Big|_{\mu^2 = k_t^2},$$

which can be adjusted by incorporating the Sudakov form factor [46–48]

$$f_g(x, k_t^2, \mu^2) \simeq \frac{\partial}{\partial k_t^2} [T_g(k_t^2, \mu^2) G(x, k_t^2)].$$

In this context, the resummation of large Sudakov logarithms like $\log(k_t/Q)$, as well as $\log(1/x)$, is applicable in the region where $Q_s \sim k_t \ll P_t \sim Q$.

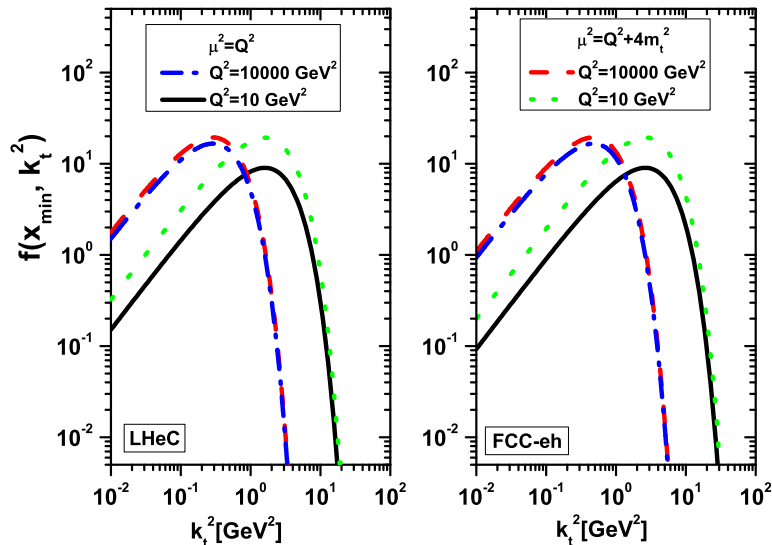


FIG. 3: UGD obtained at x_{\min} is shown at $\mu^2 = Q^2$ ($Q^2 = 10 \text{ GeV}^2$ (solid black curve) and $Q^2 = 10000 \text{ GeV}^2$ (dashed-dot blue curve)) and $\mu^2 = Q^2 + 4m_t^2$ ($Q^2 = 10 \text{ GeV}^2$ (dot green curve) and $Q^2 = 10000 \text{ GeV}^2$ (dashed red curve)) for the LHeC (left panel) and FCC-eh (right panel) COM energies as a function of k_t^2 .

The dipole cross section of the Bartels-Golec-Biernat-Kowalski (BGK) model⁴ [62] at $x_{\min} = \mu_r^2/s$ is as follows:

$$\sigma_{\text{dip}}(\mu_r^2/s, r) = \sigma_0 \left\{ 1 - \exp \left(\frac{-\pi^2 r^2 \alpha_s(\mu_r^2) x g(\mu_r^2/s, \mu_r^2)}{3\sigma_0} \right) \right\}, \quad (15)$$

where the evolution scale μ_r^2 is connected to the size r of the dipole by $\mu_r^2 = C/r^2 + \mu_0^2$ and the coefficients due to the upper bound are selected from Fit.2 in Table 3 of Ref.[44]. In the color dipole picture (CDP), the virtual photon γ^* dissociates into a $t\bar{t}$ dipole-pair which interacts with the color fields in the proton. The imaginary part of the $(t\bar{t})p$ forward scattering amplitude is defined by the dipole cross-section, $\sigma_{\text{dip}}(\mu_r^2/s, r)$ in the following form

$$\sigma_{L,T}^{\gamma^*p}(\mu_r^2/s, \mu_r^2) = \frac{1}{4\pi} \int dz d^2\mathbf{r} |\Psi_{L,T}(r, z, \mu_r^2)|^2 \sigma_{\text{dip}}(\mu_r^2/s, r), \quad (16)$$

where the γ^*p cross-sections are related to the DIS structure functions. Indeed, the DIS total scattering cross sections $\sigma_{L,T}(x, \mu^2)$ can be defined in QCD as an effective theory in the high-energy limit. This theory is known as the color glass condensate effective field theory, based on the knowledge of the incoming and outgoing elementary particles [63–66]. The longitudinal momentum fractions carried by the dipole are z and $1-z$, and the virtual wave function of the photon is defined by $\Psi_{L,T}$ according to the longitudinal and transverse photon polarizations. The kernel $|\Psi|^2$ of the light-cone wave functions in Eq. (16) based on the light-cone perturbative theory is

$$|\Psi_T^{\gamma^* \rightarrow t\bar{t}}(r, z, \mu_r^2)|^2 = \frac{2N_c \alpha_{\text{em}} e_t^2}{\pi} (m_t^2 K_0^2(\epsilon_t r) + [z^2 + (1-z)^2] \epsilon_t^2 K_1^2(\epsilon_t r)), \quad (17)$$

and

$$|\Psi_L^{\gamma^* \rightarrow t\bar{t}}(r, z, \mu_r^2)|^2 = \frac{8N_c \alpha_{\text{em}} e_t^2}{\pi} \mu^2 z^2 (1-z)^2 K_0^2(\epsilon_t r), \quad (18)$$

⁴ The dipole cross section in the BGK model is directly related to the gluon distribution and indirectly dependent on the UGD. The UGD, through a Fourier transform, is related to the gluon distribution according to the Eqs. (19), (15), (14), and (13).

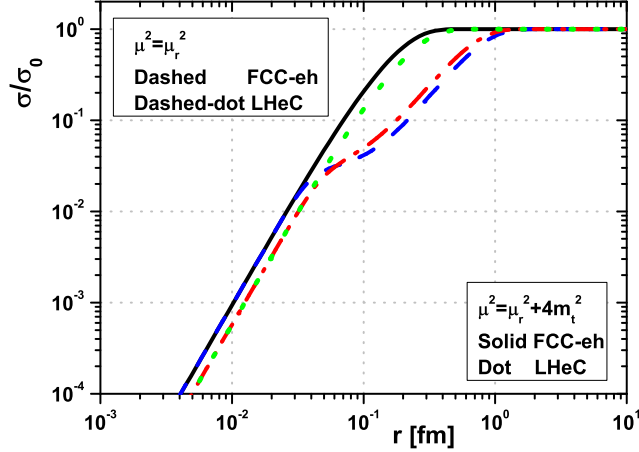


FIG. 4: The extracted ratio $\sigma_{\text{dip}}(\mu_r^2/s, r)/\sigma_0$ as a function of r at x_{min} is shown at $\mu^2 = \mu_r^2$ and $\mu^2 = \mu_r^2 + 4m_t^2$ for the LHeC and FCC-eh COM energies. LHeC: $\mu^2 = \mu_r^2$ (dashed-dot red curve) and $\mu^2 = \mu_r^2 + 4m_t^2$ (dot green curve); FCC-eh: $\mu^2 = \mu_r^2$ (dashed blue curve) and $\mu^2 = \mu_r^2 + 4m_t^2$ (solid black curve).

where N_c is the number of color charges in QCD and K_i are Bessel functions of the second kind. Here, $\epsilon_t = z(1-z)\mu^2 + m_t^2$. The effective dipole cross-section at high inelasticity is evaluated in the following form

$$\sigma_{\text{dip}}(\mu_r^2/s, r)/\sigma_0 = 1 - \exp\left(\frac{-r^2}{4}\mu_s^2\left[1 - \left(1 + \frac{\mu^2}{\mu_s^2}\right)e^{-\frac{\mu^2}{\mu_s^2}}\right]\right), \quad (19)$$

where $\mu_s^2 = (\frac{\mu^2}{sx_0})^{-\lambda}$ GeV², which depends on the the COM energies and the top-quark effective mass when $\mu^2 = \mu_r^2$ and $\mu^2 = \mu_r^2 + 4m_t^2$. In Fig.4, the results of the dipole cross-sections, $\sigma_{\text{dip}}(\mu_r^2/s, r)/\sigma_0$, of the BGK model at x_{min} are shown as a function of r at scales $\mu^2 = \mu_r^2$ and $\mu^2 = \mu_r^2 + 4m_t^2$ for the LHeC and FCC-eh COM energies. This behavior for the top quark mass is bounded based on the coefficients in the CDP. We observe that $\sigma_{\text{dip}}/\sigma_0$ is plotted as a function of the dipole size r . At the scale $\mu^2 = \mu_r^2 + 4m_t^2$ the behavior at the LHeC and FCC-eh COM energies is similar to the GBW model [43, 44, 55]. The dipole cross-sections at the scale $\mu^2 = \mu_r^2$ show a violation for $3 \times 10^{-2} \lesssim r < 1$ fm, and they exhibit the same behavior at the scale $\mu^2 = \mu_r^2 + 4m_t^2$ for the regions $r \gtrsim 1$ fm and $r \lesssim 3 \times 10^{-2}$ fm.

The DIS structure functions can be defined as an integral transform of the dipole cross section against the kernel $r\mathcal{Z}(r, \mu^2)$, which is defined by the following form [67]

$$F_{T,L}(\mu^2/s, \mu^2) = \int_0^\infty \mathcal{Z}_{T,L}(r, \mu^2)\sigma_{\text{dip}}(\mu_r^2/s, r)rdr, \quad (20)$$

where the z -integrated wave function kernel is

$$\mathcal{Z}_{T,L}(r, \mu^2) = \frac{\mu^2}{4\pi\alpha_{\text{em}}}\int_0^1 |\Psi_{T,L}^{\gamma^* \rightarrow t\bar{t}}(r, z, \mu_r^2)|^2 dz. \quad (21)$$

The ratio σ_r/F_2 at high inelasticity is defined by the following form

$$\frac{\sigma_r}{F_2}(\mu^2/s, \mu^2) = \frac{F_T}{F_T + F_L}(\mu^2/s, \mu^2) \simeq 1 - \frac{F_L}{F_T}(\mu^2/s, \mu^2) + \left(\frac{F_L}{F_T}(\mu^2/s, \mu^2)\right)^2 + \dots, \quad (22)$$

where

$$\frac{F_L}{F_T}(\mu^2/s, \mu^2) = \frac{\int_0^\infty \tilde{\mathcal{Z}}_L(r, \mu^2)\sigma_{\text{dip}}(\mu_r^2/s, r)dr}{\int_0^\infty \tilde{\mathcal{Z}}_T(r, \mu^2)\sigma_{\text{dip}}(\mu_r^2/s, r)dr}, \quad (23)$$

with $\tilde{\mathcal{Z}} \equiv r\mathcal{Z}$, where the DIS structure functions in Eq. (23) are written into a linear integral transformation of the dipole cross section. The ratio $\frac{\sigma_r^t(\mu^2/s, \mu^2)}{F_2^t}$ at the limit x_{\min} in the dipole size range $0.0001 < r < 100$ fm has a bound in the range of $\simeq 0.980$ and 0.978 for $\mu^2 = \mu_r^2$ and $\mu^2 = \mu_r^2 + 4m_t^2$ respectively at the LHeC and FCC-eh COM energies.

The LHeC and FCC-eh will explore the strange density and momentum fraction carried by top quarks, as the total cross-section of top-antitop quark pairs ($t\bar{t}$) at photoproduction is expected to be 0.05 pb at the LHeC [1]. The CP nature of the top-antitop-Higgs coupling can be analysed at the LHeC in $ep \rightarrow et\bar{t}H$ production [1, 68]. The observation of $t\bar{t}H$ production is based on a combined analysis of proton-proton collision data at COM energies of $\sqrt{s} = 7, 8,$ and 13 TeV for a Higgs boson mass of 125.09 GeV, as reported in Ref.[69]. Recently, the most model-independent direct measurement was reported in Ref.[70], with sensitivity to the top-quark Yukawa coupling. Higgs production via vector-boson fusion at the $\gamma^*g \rightarrow t\bar{t}(t\bar{t} \rightarrow H)$ will be discussed in the LHeC and FCC-eh colliders. The cross-section for this process is similar to the $gg \rightarrow t\bar{t}(t\bar{t} \rightarrow H)$ as reported in Refs.[71, 72] where the top quark loop is connected with the Higgs by the coupling $m_t(1 + \frac{H}{v})t\bar{t}$, where $v \simeq 246$ GeV is the vacuum expectation value of the Higgs field (H). These fields naturally have a mass above $2m_t$ as the top quark has a large Yukawa coupling with the Higgs boson [73]. Indeed, measuring Higgs boson production in association with a $t\bar{t}$ pair is crucial for understanding the top-quark couplings to the Higgs boson at the LHeC and FCC-eh COM energies compared to beyond-the-Standard-Model(BSM) theories [74, 75]. The cross-section for Higgs production from gluon fusion at the LHeC and FCC-eh colliders is approximately defined as:

$$\sigma(\gamma^*g \rightarrow t\bar{t}(t\bar{t} \rightarrow H)) < \frac{\alpha_{em}}{\alpha_s} \sigma(gg \rightarrow t\bar{t}(t\bar{t} \rightarrow H)). \quad (24)$$

III. RESULTS AND DISCUSSION

Determination of the strong coupling constant $\alpha_s(m_z)$ from deep-inelastic scattering and hadron collider data without a simultaneous determination of the PDFs leads to an explicit test of the partial α_s value obtained from the top quark pair production data. This value is reweighted by a factor of $N_{\text{dat}}^{\text{tot}}/N_{\text{dat}}^{t\bar{t}}$ and is estimated to be:

$$\alpha_s^{t\bar{t}}(m_z) = 0.1201 \pm 0.0012, \quad (25)$$

as reported in Ref.[76]. In the following (i.e., Figs.5-8), the DIS top structure functions at the limit $x_{\min} = Q^2/s$ in Eq. (10) depend on the gluon distribution function of Eq. (14) which is obtained from the UGD.

In Fig.5, we show the behavior of the ratio of top DIS structure functions, Eq. (10), at the limit of $x_{\min} = Q^2/s$ for $\sqrt{s} = 1.3$ and 3.5 TeV at the scales $\mu^2 = Q^2$ and $\mu^2 = Q^2 + 4m_t^2$ respectively. In Fig.5, we observe that the ratio given by Eq. (10) for F_{L2} is equal to the bound specified by Eq. (12) within the range of $10^5 < Q^2 < 10^7$ GeV². This demonstrates the importance of the longitudinal structure function of top-pair production in the LHeC and FCC-eh colliders at high inelasticity. The ratio F_{L2} shows a moderate slope at $Q^2 < 10^5$ GeV² in the scale $\mu^2 = Q^2 + 4m_t^2$. The data at small Q^2 values will span a small range of x , and this range varies strongly with μ^2 . The importance of the longitudinal structure function at large Q^2 values is shown in Fig.6. In Fig.6, the ratio σ_r/F_2 at the limit of $x_{\min} = Q^2/s$ for $\sqrt{s} = 1.3$ and 3.5 TeV at the scales $\mu^2 = Q^2$ and $\mu^2 = Q^2 + 4m_t^2$ respectively is shown. We observe that the longitudinal structure function for top-quark pair production at $Q^2 < 100$ GeV² is equal to zero. Therefore the bound in Eq. (7) for σ_r/F_2 is equal to 1 at low Q^2 values for both scales $\mu^2 = Q^2$ and $\mu^2 = Q^2 + 4m_t^2$, as we observe

$$\lim_{y \rightarrow 1} \left[\frac{\sigma_r^t(\mu^2/s, \mu^2)}{F_2^t(\mu^2/s, \mu^2)} \right] \simeq 1. \quad (26)$$

This means that at low Q^2 values (i.e., $Q^2 < 100$ GeV²) $\sigma_r^t(\mu^2/s, \mu^2) \simeq F_2^t(\mu^2/s, \mu^2)$, which determines the transversely polarized scattering at low Q^2 values.

In Fig.7, we display the behavior of the top reduced cross-section, $\sigma_r^t(\mu^2/s, \mu^2)$ at the limit of $x_{\min} = Q^2/s$ for $\sqrt{s} = 1.3$ and 3.5 TeV at the scales $\mu^2 = Q^2$ and $\mu^2 = Q^2 + 4m_t^2$. These behaviors versus of Q^2 are observable in the COM energies of new colliders. We observe that at $Q^2 < 100$ GeV² (i.e., low x values), the top reduced cross sections (and top structure functions) will be visible in the ranges $10^{-4} < \sigma_r^t < 10^{-3}$ at the scale $\mu^2 = Q^2$ and also $10^{-1} < \sigma_r^t < 1$ at the scale $\mu^2 = Q^2 + 4m_t^2$ for the LHeC and FCC-eh COM energies. We observe that the theoretical uncertainty related to the freedom in the choice of μ (i.e., $\mu^2 = Q^2$ and $\mu^2 = Q^2 + 4m_t^2$) is negligibly small at both the LHeC and FCC-eh COM energies at large Q^2 values (i.e., $Q^2 \gtrsim 4m_t^2$). However, at small Q^2 values, the uncertainties

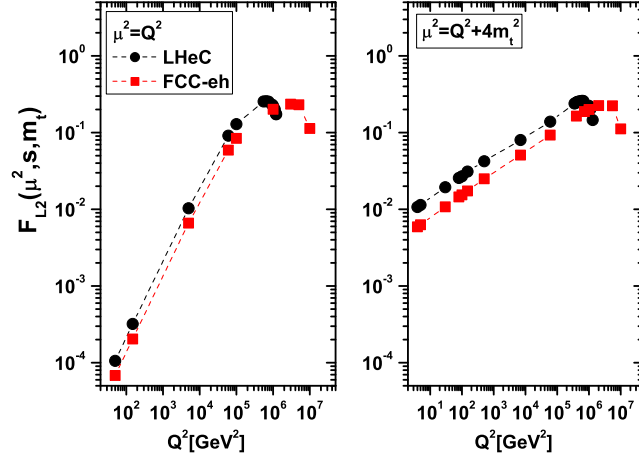


FIG. 5: The ratio $F_{L2}^t \equiv \frac{F_{L2}^t}{F_2^t}(\mu^2, s, m_t)$ as a function of Q^2 at x_{\min} is shown at $\mu^2 = Q^2$ (left panel) and $\mu^2 = Q^2 + 4m_t^2$ (right panel) for the LHeC (black circles) and FCC-eh (red squares) COM energies with $\sqrt{s} = 1.3$ and 3.5 TeV respectively.

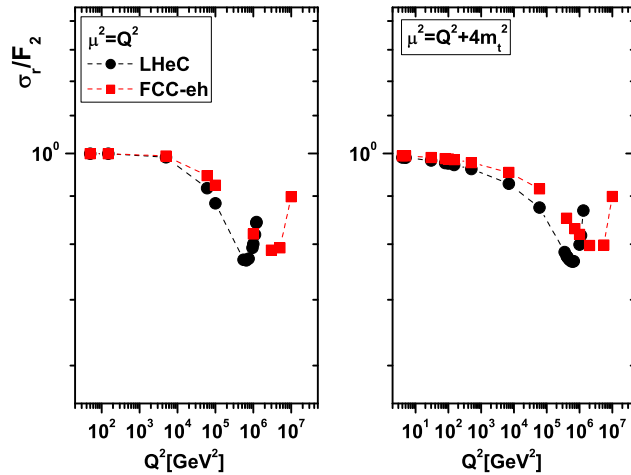


FIG. 6: The ratio $\frac{\sigma_{t\bar{t}}^t}{F_2^t}(\mu^2, s, m_t)$ as a function of Q^2 at x_{\min} is shown at $\mu^2 = Q^2$ (left panel) and $\mu^2 = Q^2 + 4m_t^2$ (right panel) for the LHeC (black circles) and FCC-eh (red squares) COM energies with $\sqrt{s} = 1.3$ and 3.5 TeV respectively.

between the results are large, as shown in Fig.7.

The behavior of the top reduced cross-section at the scale $\mu^2 = Q^2 + 4m_t^2$ at both COM energies is modified by applying the modification of the Bjorken scaling behavior. In a case where the photon wave function depends on the mass of the heavy quarks for low Q^2 , one must take into account the modification of the Bjorken variable x in high inelasticity in the following form:

$$x = \frac{Q^2}{s} + \frac{4m_t^2}{s}. \quad (27)$$

In order to assess the significance of the mass $t\bar{t}$ pair quarks in the modified Bjorken variable, we show in Fig.8 the mass dependence of the top reduced cross section at both the LHeC and FCC-eh COM energies with $\mu^2 = Q^2 + 4m_t^2$. In Fig.8, we observe that the quality of the top reduced cross-section is better if one includes the top quark mass in

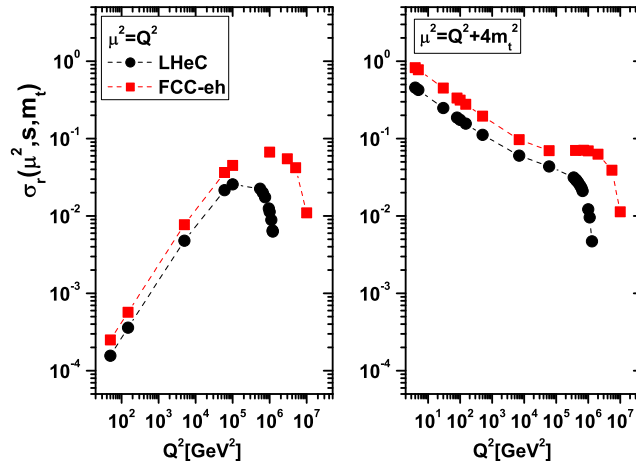


FIG. 7: The top reduced cross-section as a function of Q^2 at x_{\min} is shown at $\mu^2 = Q^2$ (left panel) and $\mu^2 = Q^2 + 4m_t^2$ (right panel) for the LHeC (black circles) and FCC-eh (red squares) COM energies with $\sqrt{s} = 1.3$ and 3.5 TeV respectively.

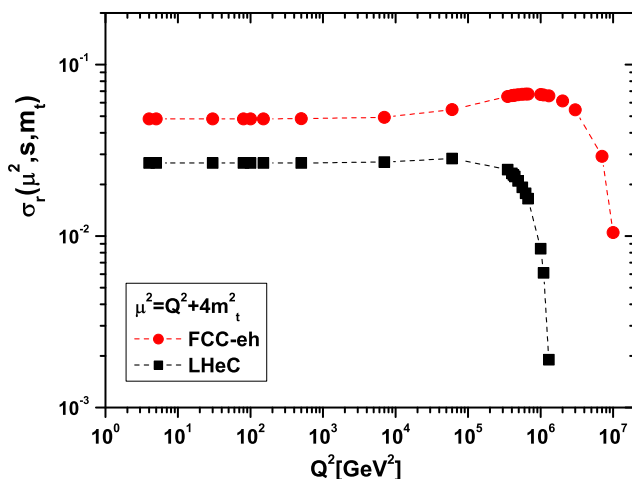


FIG. 8: The top reduced cross-section as a function of Q^2 at $x = \frac{\mu^2}{s}$ is shown at $\mu^2 = Q^2 + 4m_t^2$ for the LHeC (black circles) and FCC-eh (red squares) COM energies.

the definition of the scaling variable, as the top reduced cross-section increases as Q^2 increases. One can see that the top reduced cross-sections obtained for high inelasticity with the modified Bjorken variable are smaller and flatter than those without the effects of the top quark mass. For $Q^2 \lesssim 4m_t^2$, we observe that $\sigma_r^t \cdot s$ are approximately 0.027 and 0.049 with $\sqrt{s} = 1.3$ and 3.5 TeV respectively. On the other hand, for $Q^2 > 4m_t^2$, the behavior of σ_r^t with and without the modification of the Bjorken variable is similar. Therefore, it found to be approximately Q^2 independent in the small- Q^2 regime (i.e., $Q^2 \lesssim 4m_t^2$) as the saturation scale Q_s^2 (i.e., Fig.2) has this behavior at the scale $\mu^2 = Q^2 + 4m_t^2$. Then it continues to rise with Q^2 until reach maxima, beyond which it fall for $Q^2 \gg 4m_t^2$.

In conclusion, we have analyzed the behavior of the DIS structure function of top quark pair production at $y = 1$, where $x_{\min} = Q^2/s$, in both LHeC and FCC-eh kinematics. The ratio $\frac{F_L}{F_2}(\mu^2/s, \mu^2)$, considering the effect of the gluon density due to the UGD at the renormalization scales, is examined. This ratio with a limited bound derived

in the framework of the collinear approach, provides valuable information on the dipole picture. The dipole cross section for the production of $t\bar{t}$ in the BGK model depends on the renormalization scales at a moderate dipole size r . We demonstrate that the approximation $\sigma_r^t(\mu^2, s, m_t^2) \simeq F_2^t(\mu^2, s, m_t^2)$ is dominant for $Q^2 < 4m_t^2$ and the saturation of the dipole cross-section is valid in this domain. Finally, the top reduced cross-sections at x_{\min} for the LHeC and FCC-eh COM energies are calculated and the effects of the modification of the Bjorken scaling are applied at $\mu^2 = Q^2 + 4m_t^2$. As predicted by the authors in Ref.[20], a TeV ep-collider (i.e., LHeC and FCC-eh colliders) will provide the exact pair production rate into WW approximation. Therefore, the LHeC and FCC-eh should certainly consider the longitudinal structure function for top production at $Q^2 \gtrsim 4m_t^2$ as an important item on the list of physics topics.

-
- [1] P. Agostini et al. (LHeC Collaboration and FCC-eh Study Group), J. Phys. G **48**, 110501 (2021).
[2] A. Abada, et al., FCC Collaboration, Eur. Phys. J. C **79**, 474 (2019).
[3] M. Klein, arXiv[hep-ph]:1802.04317; Ann. Phys. **528**, 138 (2016).
[4] S.J. Brodsky, SLAC-PUB-14487, CERN-LHeC-Note-2011-002 PHY, arXiv[hep-ph]:1106.5820; H. Sun, arXiv[hep-ph]:1710.06260; H. Denizli, et al., Phys. Rev. D **96**, 015024 (2017).
[5] M.Gao and J.Gao, Phys. Rev. D **104**, 053005 (2021).
[6] V.A.Okorokov, J. Phys.: Conf. Ser. **1690**, 012006(2020), arXiv[hep-ph]:2010.03912.
[7] O.B.Bylund, arXiv[hep-ex]:2103.14772.
[8] E.R.Nocera, M.Ubiali and C.Voisey, JHEP **05**, 067 (2020).
[9] CMS Collaboration, Eur.Phys.J.C **79**, 368 (2019); Phys. Rev. D **93**, 072004 (2016).
[10] ATLAS Collaboration, Phys. Lett. B **810**, 135797(2020); Eur. Phys. J. C **79**, 290 (2019).
[11] R.Barcelo, Proceedings of Second Young Researchers Workshop "Physics Challenges in the LHC era", Frascati Physics Series LI (2010) 13-18, arXiv[hep-ph]:1006.1219.
[12] S.Catani et al., TIF-UNIMI-2022-15, ZU-TH 46/22, MPP-2022-128, PSI-PR-22-30, arXiv[hep-ph]:2210.07846.
[13] S.Devoto et al., ZU-TH-57/24, PSI-PR-24-22, TUM-HEP-1538/24, arXiv[hep-ph]:2411.15340.
[14] N.Kidonakis and N.Yamanaka, arXiv[hep-ph]: 2509.23293.
[15] Tie-Jiun Hou et al., Phys.Rev.D**103**, 014013(2021).
[16] G.R.Boroun, Phys.Lett. B**744**, 142(2015).
[17] G.R.Boroun, Phys.Lett. B**838**, 137712(2023); B.Rezaei and G.R. Boroun, Europhysics Letters**130**, 51002 (2020).
[18] G.R.Boroun, Phys.Lett. B**741**, 197(2015).
[19] Gerhard A. Schuler, Nucl. Phys. B **299**, 21 (1988).
[20] U. Baur, J.J. van der Bij, Nucl. Phys. B **304**, 451 (1988).
[21] M. Drees, K. Grassie, Z. Phys. C **28**, 451 (1985).
[22] M. Gluck, E. Reya, Phys. Lett. B **83**, 98 (1979).
[23] L.M. Jones, H.W. Wyld, Phys. Rev. D **17**, 759 (1978).
[24] N.Ya. Ivanov, Nucl. Phys. B **814**, 142 (2009); N.Ya. Ivanov and B.A.Kniehl, Eur.Phys.J.C **59**, 647 (2009).
[25] R.D. Ball et al., [NNPDF Collaboration], Eur. Phys. J. C **77**, 663(2017).
[26] F. Demartin et al., Phys. Rev. D **82**, 014002 (2010).
[27] J.L.A. Fernandez et al., [LHeC Study Group], J. Phys. G: Nucl. Part. Phys. **39**, 075001 (2012).
[28] Y.Kitadono, Phys.Lett. B**702**, 135(2011).
[29] W.L.van Neerven, Acta Physica Polonica B **28**, 2715 (1997).
[30] A.V. Kotikov, G. Parente, Nucl. Phys. B **549**, 242 (1999).
[31] A.Yu. Illarionov, A.V. Kotikov, G. Parente, Phys. Part. Nucl. **39**, 307 (2008); A.Yu. Illarionov, B.A.Kniehl, and A.V. Kotikov, Phys. Lett.B **663**, 66 (2008).
[32] L. Mankiewicz, A. Saalfeld, T. Weigl, Phys. Lett. B **393**, 175 (1997).
[33] A.V.Kotikov, A.V.Lipatov and P.Zhang, Phys. Rev. D **104**, 054042 (2021).
[34] G.R.Boroun, Eur. Phys. J. Plus **138**, 252 (2023).
[35] G.R.Boroun, Phys.Rev.D **109**, 054012 (2024).
[36] Frank E. Taylor, Phys. Rev. D **111**, 052001 (2025).
[37] G.R.Boroun, Phys.Rev.D **112**, 074022 (2025).
[38] EIC BNL, <https://www.bnl.gov/eic/>.
[39] C.Ewerz et al., Phys.Lett.B **720**, 181 (2013).
[40] M.Niedziela and M.Praszalowicz, Acta Physica Polonica B **46**, 2018 (2015).
[41] G.S.Ramos and M.V.T.Machado, Phys.Rev.D **101**, 074040 (2020).
[42] A. Accardi et al., Eur. Phys. J. A **52**, 268 (2016).
[43] K. J. Golec-Biernat and M. Wusthoff, Phys. Rev. D **60**, 114023(1999).
[44] K. Golec-Biernat and S. Sapeta, J. High Energy Phys. **03**, 102 (2018).
[45] D.A.Fagunders and M.V.T.Machado, Phys.Rev.D **107**, 014004 (2023).

- [46] M.A. Kimber, A.D. Martin, M.G. Ryskin, Phys. Rev. D **63**, 114027 (2001); A.D. Martin, M.G. Ryskin, G. Watt, Eur. Phys. J. C **31**, 73 (2003); A.D. Martin, M.G. Ryskin, G. Watt, Eur. Phys. J. C **66**, 163 (2010).
- [47] T.Goda, K.Kutak, and S.Sapeta, IFJPAN-IV-2023-2, arXiv[hep-ph]: 2305.14025.
- [48] G.R.Boroun, Phuoc Ha, A.V.Kotikov, and A.V.Lipatov, arXiv [hep-ph]:2510.14678.
- [49] N. N. Nikolaev and B. G. Zakharov, Phys. Lett. B **332**, 184 (1994).
- [50] N. N. Nikolaev and W. Schafer, Phys. Rev. D **74**, 014023 (2006).
- [51] I.P.Ivanov and N.N.Nikolaev, Phys.Rev.D **65**, 054004 (2002).
- [52] I.V. Anikin et al., Phys. Rev. D **84**, 054004 (2011).
- [53] M. Hentschinski, A. Sabio Vera and C. Salas, Phys. Rev. Lett. **110**, 041601 (2013).
- [54] G. Watt, A.D. Martin and M.G. Ryskin, Eur. Phys. J. C **31**, 73 (2003).
- [55] K.Golec-Biernat and M.Wusthoff, Phys. Rev. D **59**, 014017 (1998).
- [56] A.D. Bolognino, A. Szczurek and W. Schafer, Phys. Rev. D **101**, 054041 (2020).
- [57] A.D. Bolognino et al., Eur.Phys.J.C **78**, 1023 (2018).
- [58] A.D. Bolognino et al., Eur.Phys.J.C **81**, 846 (2021).
- [59] G.R.Boroun, Eur. Phys. J. C **84**, 960 (2024).
- [60] G.R. Boroun, Eur.Phys.J.A **60**, 3 (2024).
- [61] Y. Afik and J. R. M. de Nova, Eur. Phys. J. Plus **136**, 907 (2021).
- [62] J.Bartels, K.Golec-Biernat and H.Kowalski, Phys. Rev. D **66**, 014001 (2002).
- [63] A. Morreale and F. Salazar, Universe **7**, 312 (2021).
- [64] H. Weigert, Prog. Part. Nucl. Phys. **55**, 461 (2005).
- [65] F. Gelis, E. Iancu, J. Jalilian-Marian, and R. Venugopalan, Annu. Rev. Nucl. Part. Sci. **60**, 463 (2010).
- [66] J. L. Albacete and C. Marquet, Prog. Part. Nucl. Phys. **76**, 1 (2014).
- [67] H.Hanninen, A.Kykanen and H.Schluter, Phys.Rev.D **112**, 094026 (2025).
- [68] B. Coleppa, M. Kumar, S. Kumar, and B. Mellado, Phys. Lett. B **770**, 335(2017).
- [69] A.M.Sirunyan et al., Phys.Rev.Lett.**120**, 231801 (2018).
- [70] ATLAS Collaboration, CERN-EP-2025-216, arXiv [hep-ex]: 2509.16039.
- [71] F.Maltoni, $pp \rightarrow \text{Higgs}$: a case study, GIF School, September 2007.
- [72] P.Bolzoni, F.Maltoni, Sven-Olaf Moch, and M.Zaro, Phys.Rev.Lett.**105**, 011801 (2010).
- [73] R.Barcelo, Proceedings of Second Young Researchers Workshop "Physics Challenges in the LHC era", Frascati Physics Series LI (2010) 13-18 , arXiv [hep-ph]:1006.1219.
- [74] Ana Elena Dumitriu, "XXVII International Workshop on Deep-Inelastic Scattering and Related Subjects- DIS2019" PoS(DIS2019)086.
- [75] H.Hesari, H.Khanpour, and M.Mohammadi Najafabadi, Phys.Rev.D**97**, 095041 (2018).
- [76] S.Forte, J.Rojo and R.Stegeman, The European Physical Society Conference on High Energy Physics (EPS-HEP2025) 7-11 July 2025, arXiv[hep-ph]: 2511.22561.